Nature Environment and Pollution Technology
An International Quarterly Scientific Journal

p-ISSN: 0972-6268
(Print copies up to 2016)
e-ISSN: 2395-3454

Vol. 21 | No. 2 | pp. 421-432 | 2022

Original Research Paper

https://doi.org/10.46488/NEPT.2022.v21i02.001

Open Access Journal

Geochemical Characteristics and Geological Significance of Cassiterite in the Dalong Tin Deposit, Baoshan Block, SW China

Chuanyu Zhang*(**), Wanting Li*, Haijun Yu**†, Yingxiang Lu**, Jianze Sha** and Shusheng Yang****

*Faculty of Land Resource Engineering, Kunming University of Science and Technology, Kunming, 650093, China

**MLR Key Laboratory of Sanjiang Metallogeny and Resources Exploration and Utilization, Yunnan Geological Survey, Kunming, 650051, China

***School of Earth Science, Yunnan University, Kunming, 650500, China

†Corresponding author: Haijun Yu; yhj307@163.com

Nat. Env. & Poll. Tech.
Website: www.neptjournal.com

Received: 08-05-2021
Revised: 07-07-2021
Accepted: 25-07-2021

Key Words:
Cassiterite
Trace element
Deposit type
Dalong tin deposit

ABSTRACT

The Dalong tin deposit, located in the Luziyuan polymetallic ore field of the southern Baoshan block, Southwest China, is composed of lenticular and bedded orebodies hosted in a Cambrian slate-marble sequence. As the only tin deposit in the orefield, the genesis of the Dalong deposit is of great significance to the understanding of regional metallogenic regularity. Based on a systematic field survey and petrographic observation, EPMA and LA-ICP-MS major/trace element analyses of cassiterite were carried out in this study. The enrichment of Fe, W, and Ti in cassiterite, as well as the depletion of Nb, Ta, and Mn, reveal cassiterite's features in granitic magmatic-hydrothermal deposits. The Dalong deposit can be categorized as a magmatic-hydrothermal vein-type deposit because of its sulfur isotopic properties, and the main sources of ore-forming fluid and minerals are thought to be buried intermediate-acid intrusions in the mining area's depths.

INTRODUCTION

The Baoshan block is located in the southern section of Sanjiang Tethys, where several large-giant lead-zinc polymetallic deposits (such as the Luziyuan, Hetaoping, Jinchanghe, Xiyi, Meng xing deposits) with total resources of more than 8 Mt Zn + Pb (Gao et al. 2016), as well as dozens of small- to medium-sized deposits have been discovered in recent years, making it one of the most important polymetallic mineralization areas in Southwest China (Fig. 1). The Dalong tin deposit is located in the Luziyuan ore field at the southern end of the Baoshan block, followed by Luziyuan iron-lead-zinc polymetallic deposit, Shuitoushan lead-zinc deposit, Fangyangshan copper-lead-zinc deposit, and Xiaogangou gold deposit, from the center to the periphery, showing good mineralization temperature zoning and great prospecting potential. However, as an important deposit in the orefield, research on the Dalong tin deposit is currently mainly concentrated on the geological characteristics of the deposit (Cheng et al. 2006, Xie & Liang 2018), instead of the trace elements of cassiterite & the genesis of the deposit. This has greatly restricted the understanding of metallogenetic regularity of the Luziyuan ore field and even the Baoshan block.

Cassiterite (SnO_2), the most important tin ore mineral, can form both in magmatic and hydrothermal systems over broad P-T conditions. Due to its refractory properties, cassiterite is resistant to post hydrothermal disturbances (Plimer et al. 1991, Jiang et al. 2004). Therefore, trace elements in cassiterite are taken as an indicator to fingerprint the source of ore-forming fluids and physico-chemical conditions of mineralization processes (Schneider et al. 1978, Murciego et al. 1997, Hennigh & Hutchinson 1999). In recent years, with the development of modern microanalytical techniques, the in-situ laser-ablation inductively coupled mass spectroscopy (LA-ICP-MS) has been successfully applied to determining trace element content in cassiterite (Wang et al. 2014a, Guo et al. 2018a, 2018b, Chen et al. 2019, Cheng et al. 2019, Fei et al. 2020, Liu et al. 2021, Gemmrich et al. 2021), which greatly improves the efficiency and precision of this test. In this paper, based on previous studies and combined with field geological survey and geological characteristics observation of the deposit, we carried out EPMA and LA-ICP-MS analyses on major and minor/trace elements of cassiterite in the Dalong deposit, and also make a comparison of reported sulfur isotope characteristics between Dalong deposit and other typical deposits in the Baoshan block. After these, we discussed (1) the trace elements substitution mechanism in

cassiterite; (2) the genesis of cassiterite; (3) the source of sulfur in the Dalong deposit. These results are helpful to better understand the origin of the Dalong deposit and the metallogenic mechanism of the Luziyuan orefield.

GEOLOGICAL SETTING

On the east side of the India-Eurasia collision zone is the Baoshan block (Fig. 1a). It is a distinct terrane from the Gondwana continent that formed part of the Sibumasuterrane in the Late Paleozoic (Metcalfe 2011). The Nujiang fault and the Lancangjiang fault define the western and eastern boundaries of the Baoshan block, respectively, but the north section of it is lost in the Bijiang area due to the convergence of the two faults (Tao et al. 2010). The Gongyanghe Group formed from Neoproterozoic to Middle Cambrian constitutes the metamorphic basement of the Baoshan block, which is covered by a set of shallow to semi-deep marine clastic rocks and carbonate rocks and siliceous rocks formed from Late Cambrian to Mesozoic. The structural deformation in the region is characterized by the development of densely arranged faults and folds. The structural lines are mainly distributed in the SN, NW, and NE directions, and are generally curved toward the east. Frequent magmatic activities are dominated

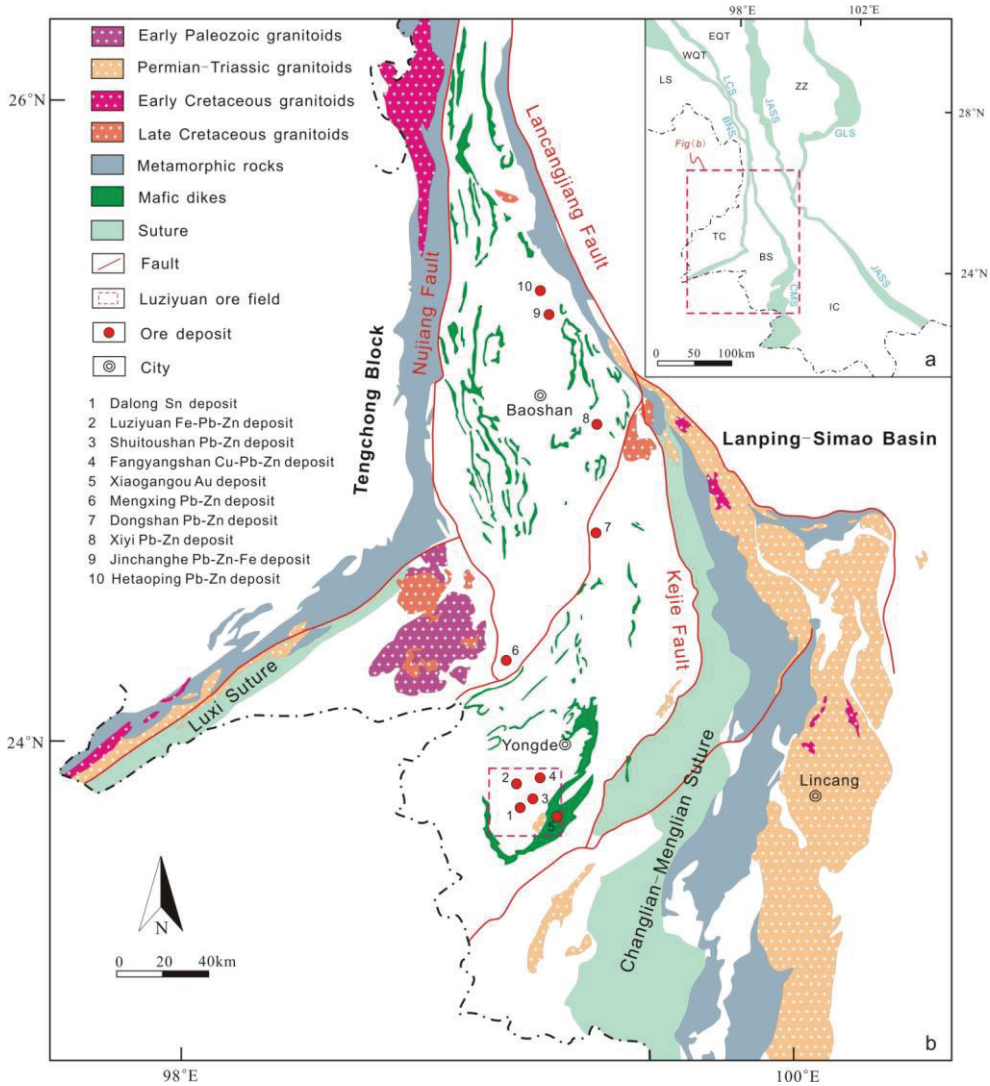

Fig. 1: **a** Tectonic setting of Baoshan block (after Deng et al. 2014, Wang et al. 2014b); **b** Geological sketch map showing the regional tectonic framework of the Baoshan block and the distribution of sedimentary and igneous units (after Deng et al. 2014, Liao et al. 2015, Li et al. 2015). BNS = Bangong - Nujiang suture, BS = Baoshan block, CMS = Changning - Menglian suture, EQT = East Qiangtang terrane, GLS = Garze - Litang suture, IC = Indochina block, LCS = Lancang suture, LS = Lhasa terrane, SC = South China block, TC = Tengchong block, WQT = West Qiangtang terrane, ZZ = Zhongza block.

by intermediate-acid intrusive rocks and are mainly concentrated in the Early Paleozoic and Mesozoic in the Baoshan block (Fig. 1b). Among them, the Early Paleozoic granites are mainly distributed in the central and southern Baoshan block, with an age range roughly between 502Ma and 448 Ma, during the unification Gondwanaland period (Chen et al. 2007, Liu et al. 2009, Dong et al. 2013), while outcrops of Mesozoic granites are mainly exposed on the edge of the Baoshan block (Muchang alkali granite: 266 ± 5.4 Ma (Ye et al. 2010); Gengma monzogranite: 232-221Ma (Nie et al. 2012); Zhibenshan granite: 127 ± 1.6Ma (Tao et al. 2010); Kejie granite: 93 ± 13Ma (Tao et al. 2010); Bangmiao granite: 83-85Ma (Dong et al. 2013).

The first, second, third, and fourth members of the Upper Cambrian Baoshan Formation, all striking NE and dipping NW are exposed strata in the Dalong mining district. The Sn orebodies are mostly found in the limestone or slate of the Baoshan Formation's later three members (Fig. 2a).

The principal fold structure in this area is the Wumulan anticline, which runs in an NNE direction and has the Dalong deposit on its NW limb. The fault structures primarily trend NE, NW, and nearly SN. The main storage of tin ore bodies is on the NE and NW-trending faults, as well as their subsidiary EW-trending interlayer fracture zone, whereas the approximately SN-trending faults crosscut both the earlier faults and orebodies. Magmatic rocks can be scarcely found in the Dalong ore district, nevertheless, both regional gravity anomalies and airborne magnetic surveys have inferred a concealed intermediate-acid intrusion distributed within about 300km^2 in the deep of the Dalong ore district. (Jiang et al. 2013, Liang et al. 2015).

The Dalong deposit is composed of 11 tin orebodies, which are mainly struck between 240 ^{o} and 290 ^{o} with dip angles of 35-60º. The orebodies are generally 40 to 500m long and 0.65 to 2.65m thick (Fig. 2b). Furthermore, the orebodies are mostly stratified and locally lenticular in shape, with the characteristics of expansion, contraction, and pinching out along the strike and tendency, which are controlled by faults. The ores are mainly hosted in quartz veins, the tin grade ranges from 0.11% to 4.97%, with an average of 0.63%. Mineral assemblages are relatively simple in the

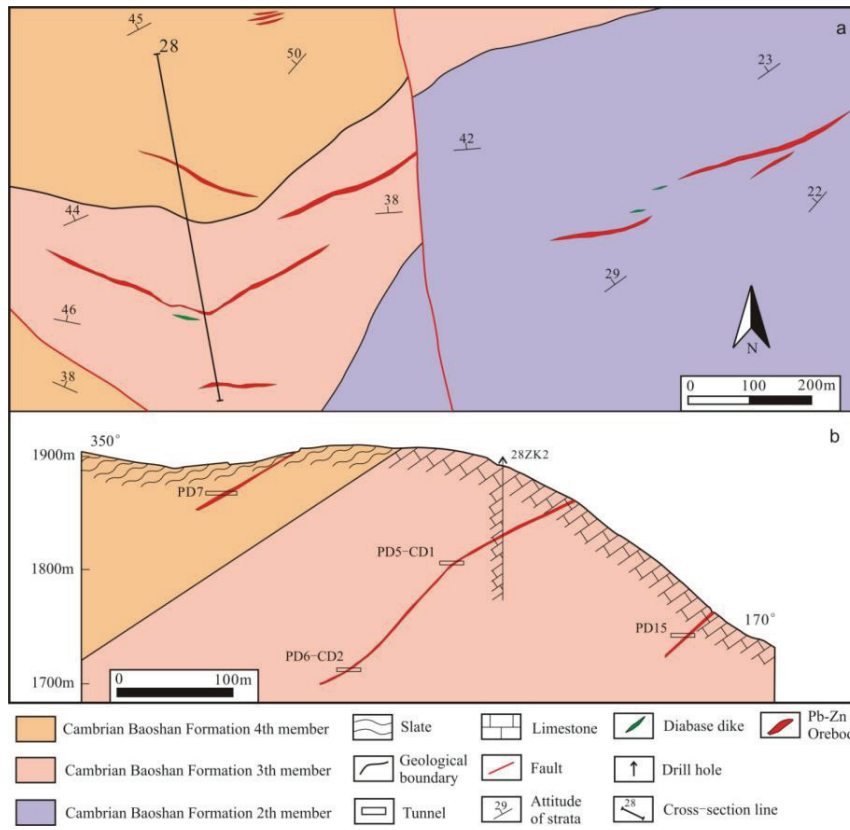

Fig. 2: **a** Geological sketch map of the Dalong deposit (modified after Cheng et al. 2006); **b** Geological section along the Number 28 exploration line in the Dalong deposit

deposit. The metallic minerals are mainly cassiterite, pyrite, chalcopyrite, arsenopyrite, limonite, with minor pyrite, tetrahedrite, sphalerite (Fig 3(a-d)), the nonmetallic minerals mainly include quartz, sericite, and calcite. The ores appear as disseminated, vein, veinlet, stockwork, or honeycomb (Fig 3b), and geodes are commonly observed (Fig 3a). The main textures of the ore include euhedral-subhedral (Fig. 3a-b), cataclastic and metasomatic residual textures. Alteration types- include silicification, pyritization, monetization, and weak sericitization.

Cassiterite in the Dalong deposit is mostly brown to dark brown and occurs in euhedral-subhedral granular aggregates coexisting with quartz (Fig 3(a-b), e). The cassiterite crystals are mainly short columnar shaped, with variable grain sizes (1-15mm in diameter), except that some grains have obvious cracks and broke into irregular shapes (Fig. 3c). Dissolution occurs on the edge of some cassiterite, mostly in a zigzag or harbor shape, and a typical zonal structure is occasionally developed in some cassiterite, suggested by alternating bright and dark rings in the cathodoluminescence (CL) images (Fig. 3f).

MATERIALS AND METHODS

Samples for this study were collected from adits in the Dalong deposit. After being separated from ore samples, large cassiterite grains with the least cracks and inclusions were chosen by hand under a binocular microscope, mounted in epoxy resin, and polished to expose the interior surface. Major compositions of cassiterite were determined by EPMA (JEOL JXA-8230) at Wuhan Sample Solution Analytical Technology Co. Ltd. The accelerating voltage was 15 kV, and the sample current was 5×10^{-8}A with a 1 μm probe diameter. In situ trace, elemental analyses were performed using an iCAPRQ ICP-MS coupled with an NWR 193nm laser, in the Guangzhou Tuoyan Testing Technology Co. Ltd. Cassiterite grains were analyzed using a laser energy density of 5J.cm^{-2}, a spot size of 50μm, and a laser pulse rate of 6Hz. Helium was used as a carrier gas and was mixed with argon via a Y-connector before entering the ICP-MS. Each spot analysis incorporated a background acquisition of approximately 50s followed by 45s of sample data acquisition. The contents of trace elements for unknown samples were corrected based on the external calibration material NISTSRM 610.

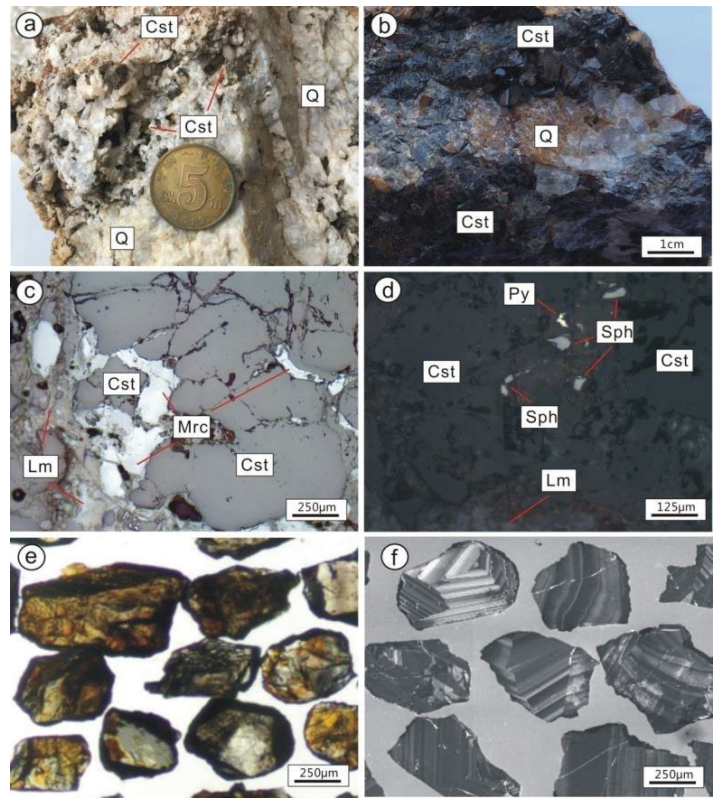

Fig. 3: The micrograph and CL image in the Dalong deposit. **a** Brown cassiterite-quartz geode in quartz vein; **b** Massive cassiterite ore. The cassiterite is dark brown, coarse-grained, euhedral, and associated with quartz; **c** Cassiterite is metasomatized by marcasite and limonite along with fractures and grain boundaries; **d** Cassiteriteis associated with pyrite and sphalerite; **e** Cassiterite grains under transmitted light; **f** The clear zonal structure in cassiterite under cathodoluminescence (CL). Cst-cassiterite; Lm-limonite; Mrc-marcasite; Py-pyrite; Sp-sphalerite; Q-quartz

RESULTS

Results of EPMA analysis of major elements in cassiterite from Dalong deposit are shown in Table 1. The content of SnO_2, FeO and TiO_2 in cassiterite is 98.32 - 100.11wt%, 0.01 - 0.08 wt %, and 0.02- 0.57 wt %, respectively, with a negative correlation between TiO_2 and SnO_2(Fig. 4a). It is suggested that Ti can enter the cassiterite crystal lattice via a simple bivalent cation substitution of $Ti^{4+} \leftrightarrow Zn^{2+}$, which is also confirmed by the time-resolved LA-ICP-MS depth profiles observed in this study (Fig. 5). Cassiterite grains are relatively depleted in Nb (0.73-67 ppm), Ta (0-1.11ppm), Mn (0.11-8ppm), Sc (2-23 ppm), Zr (0.05-61 ppm), and Hf (0.01-5ppm), and rich in Ti (480-4299ppm), Fe (69-899 ppm) and W (640-3414ppm), revealed by in-situ LA-ICP-MS analyses (Table 2). There are clear positive correlations between Zr and Hf, Nb and Ta, V and Sc, as shown in Figure 6. The Co and Ni concentrations are usually steady in the

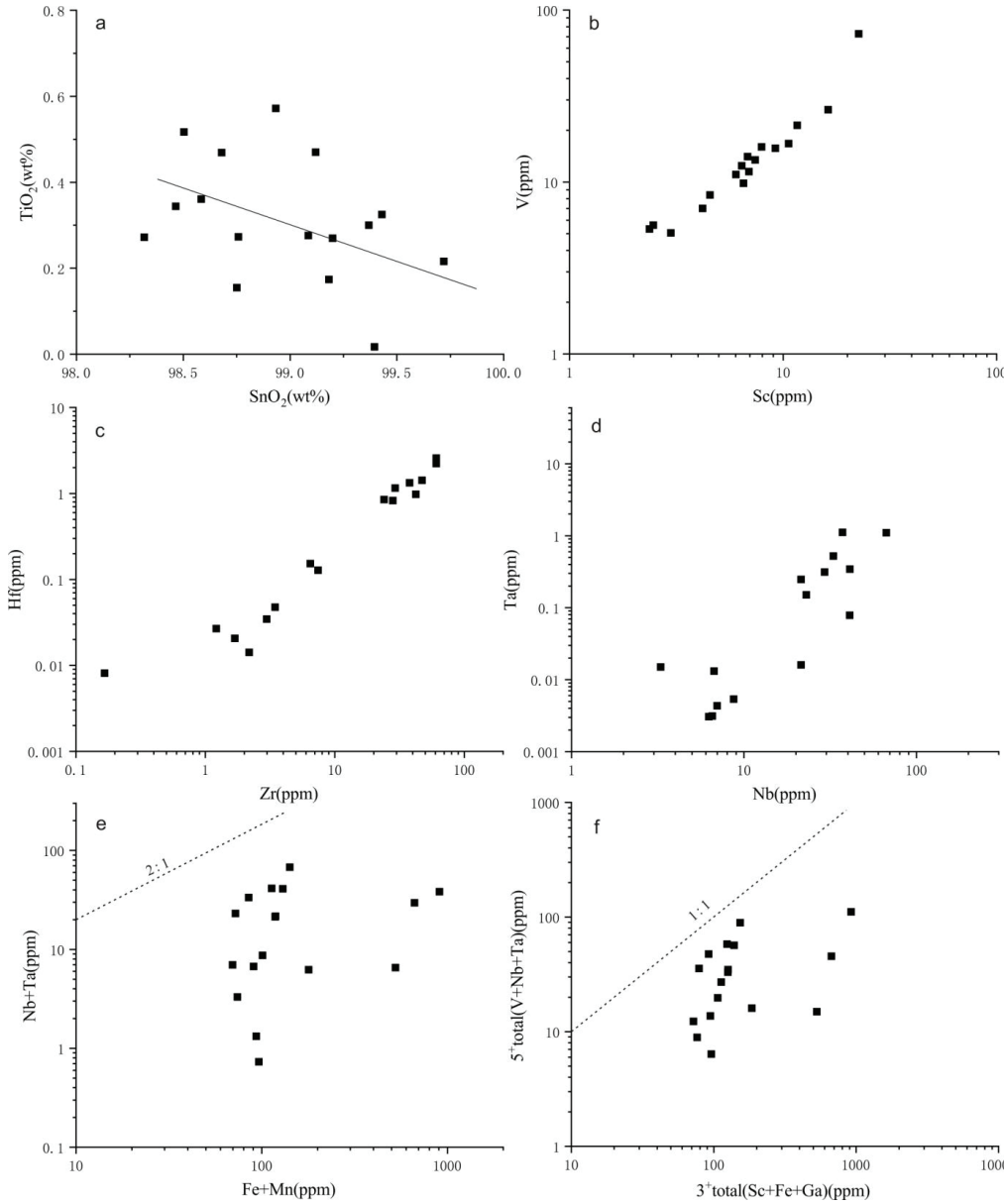

Fig. 4: Binary plots of (a) TiO_2 vs. SnO_2, (b) V vs. Sc, (c) Hf vs. Zr, (d) Ta vs. Nb, (e) Nb+Ta vs. Fe+Mn, (f) V+ Nb+Ta vs. Sc+Fe+Ga in cassiterites from the Dalong deposit.

Table 1: Major element compositions (wt.%) of cassiterite by EPMA from the Dalong deposit.

Spots	DL7-1	DL7-2	DL7-3	DL7-4	DL7-5	DL7-6	DL7-7	DL7-8	DL7-9	DL7-10	DL7-11	DL7-12	DL7-13	DL7-14	DL7-15	DL7-16	DL7-17
TiO_2	0.22	0.52	0.57	0.34	0.33	0.36	0.30	0.47	0.27	0.47	0.27	0.27	0.17	0.28	0.09	0.16	0.02
SnO_2	99.72	98.50	98.93	98.47	99.43	98.58	99.37	99.12	99.20	98.68	98.32	98.76	99.18	99.09	100.11	98.75	99.40
Nb_2O_5	0.00	0.00	0.01	0.00	0.01	0.00	0.00	0.00	0.04	0.00	0.00	0.01	0.02	0.03	0.01	0.02	0.01
ZrO_2	0.01	0.00	0.09	0.01	0.10	0.00	0.00	0.00	0.05	0.00	0.00	0.02	0.02	0.02	0.00	0.06	0.00
Al_2O_3	0.00	0.00	0.00	0.01	0.00	0.00	0.00	0.00	0.01	0.00	0.00	0.00	0.00	0.00	0.01	0.00	0.00
Cr_2O_3	0.00	0.00	0.00	0.03	0.03	0.00	0.01	0.01	0.03	0.00	0.01	0.02	0.00	0.00	0.00	0.00	0.01
MnO	0.00	0.01	0.04	0.01	0.00	0.00	0.00	0.02	0.02	0.00	0.00	0.00	0.00	0.00	0.00	0.00	0.01
FeO	0.00	0.02	0.00	0.03	0.02	0.08	0.00	0.07	0.04	0.05	0.06	0.05	0.00	0.04	0.01	0.02	0.03
HfO_2	0.00	0.00	0.10	0.04	0.00	0.00	0.03	0.00	0.06	0.01	0.00	0.00	0.00	0.05	0.00	0.04	0.00
MgO	0.01	0.01	0.01	0.01	0.01	0.00	0.01	0.00	0.01	0.00	0.04	0.00	0.02	0.00	0.00	0.00	0.02
Ta_2O_5	0.04	0.03	0.18	0.05	0.05	0.00	0.08	0.07	0.04	0.08	0.10	0.03	0.09	0.05	0.01	0.04	0.05
WO3	0.00	0.10	0.12	0.00	0.00	0.00	0.00	0.00	0.00	0.00	0.00	0.00	0.01	0.00	0.00	0.00	0.00
Total	99.99	99.20	100.06	99.01	99.98	99.02	99.81	99.76	99.77	99.28	98.79	99.15	99.52	99.55	100.24	99.09	99.55
base on 4 oxygen																	
Ti	0.008	0.020	0.021	0.013	0.012	0.014	0.011	0.018	0.010	0.018	0.010	0.010	0.007	0.010	0.003	0.006	0.001
Sn	1.991	1.977	1.968	1.982	1.982	1.985	1.986	1.979	1.983	1.980	1.985	1.987	1.990	1.986	1.995	1.990	1.996
Nb	0.000	0.000	0.000	0.000	0.000	0.000	0.000	0.000	0.001	0.000	0.000	0.000	0.001	0.001	0.000	0.001	0.000
Zr	0.000	0.000	0.002	0.000	0.002	0.000	0.000	0.000	0.001	0.000	0.000	0.000	0.000	0.000	0.000	0.002	0.000
Al	0.000	0.000	0.000	0.001	0.000	0.000	0.000	0.000	0.001	0.000	0.000	0.000	0.000	0.000	0.001	0.000	0.000
Cr	0.000	0.000	0.000	0.001	0.001	0.000	0.000	0.000	0.001	0.000	0.000	0.001	0.000	0.000	0.000	0.000	0.000
Mn	0.000	0.000	0.002	0.001	0.000	0.000	0.000	0.001	0.001	0.000	0.000	0.000	0.000	0.000	0.000	0.000	0.001
Fe	0.000	0.001	0.000	0.001	0.001	0.003	0.000	0.003	0.002	0.002	0.003	0.002	0.000	0.002	0.000	0.001	0.001
Hf	0.000	0.000	0.001	0.001	0.000	0.000	0.000	0.000	0.001	0.000	0.000	0.000	0.000	0.001	0.000	0.001	0.000
Mg	0.001	0.001	0.001	0.001	0.000	0.000	0.001	0.000	0.001	0.000	0.003	0.000	0.001	0.000	0.000	0.000	0.001
Ta	0.001	0.000	0.002	0.001	0.001	0.000	0.001	0.001	0.001	0.001	0.001	0.000	0.001	0.001	0.000	0.001	0.001
W	0.000	0.001	0.002	0.000	0.000	0.000	0.000	0.000	0.000	0.000	0.000	0.000	0.000	0.000	0.000	0.000	0.000
total	2.000	1.999	1.998	2.002	2.001	2.002	2.000	2.002	2.002	2.001	2.002	2.001	2.000	2.000	2.000	2.000	2.001
Nb+Ta	0.001	0.000	0.003	0.001	0.001	0.000	0.001	0.001	0.001	0.001	0.001	0.001	0.002	0.001	0.001	0.001	0.001
Fe+Mn	0.000	0.001	0.002	0.002	0.001	0.003	0.000	0.004	0.003	0.002	0.003	0.002	0.000	0.002	0.000	0.001	0.002

Table 2: Trace element compositions (ppm) of cassiterite by LA-ICP-MS from the Dalong deposit.

Spots	DL7-1	DL7-2	DL7-3	DL7-4	DL7-5	DL7-7	DL7-8	DL7-9	DL7-11	DL7-12	DL7-13	DL7-14	DL7-16	DL7-17	DL7-18	DL7-19	DL7-20
Sc	2.37	2.47	6.53	6.40	16.24	7.94	2.98	6.01	6.92	11.65	22.60	6.83	4.55	10.61	4.20	7.39	9.21
Ti	631	708	1853	2932	888	3263	481	1822	2436	4299	3335	3186	1268	3606	1134	2044	3456
V	5.32	5.61	9.82	12.44	26.32	16.02	5.06	11.05	11.49	21.39	72.74	14.04	8.40	16.73	7.02	13.44	15.72
Cr	0.118	0.930	0.249	0.000	0.011	0.591	0.171	0.000	0.548	1.419	5.133	0.000	0.488	0.750	0.371	0.180	0.272
Mn	0.257	0.108	0.867	0.035	0.308	2.886	0.555	0.428	0.125	0.407	8.401	0.124	0.695	0.163	0.149	0.127	0.315
Fe	69.4	73.8	178.0	72.2	96.3	662.2	92.9	100.5	118.7	141.0	898.7	85.0	523.9	113.0	90.2	118.2	129.6
Co	5.77	5.884	5.65	5.48	5.74	5.86	5.66	5.44	5.36	5.65	5.62	5.42	5.46	5.36	5.27	5.24	5.060
Ni	42.22	42.05	42.15	42.29	41.95	41.23	42.48	41.03	40.60	39.78	40.19	40.62	40.27	40.42	39.55	39.35	38.06
Cu	0.315	0.612	0.527	0.627	0.128	3.055	0.264	0.649	0.519	0.387	3.679	5.612	4.130	0.047	0.379	0.012	0.454
Zn	0.552	0.023	1.195	0.098	0.049	9.036	0.998	0.212	0.979	0.305	11.197	0.085	5.434	0.132	0.445	0.039	0.584
Ga	0.081	0.177	0.169	0.145	0.211	0.254	0.141	0.178	0.114	0.179	0.420	0.169	0.201	0.217	0.209	0.306	0.160
Rb	0.000	0.016	0.000	0.014	0.000	0.000	0.019	0.001	0.000	0.005	0.094	0.014	0.000	0.009	0.000	0.029	0.008
Sr	0.015	0.004	0.009	0.008	0.053	0.098	0.021	0.050	0.045	0.024	1.330	0.000	0.127	0.009	0.003	0.011	0.028
Zr	1.21	6.47	2.18	28.12	0.04	37.80	0.17	2.98	24.03	60.80	29.31	60.84	1.69	47.21	3.45	7.43	42.18
Hf	0.027	0.153	0.014	0.830	0.000	1.331	0.008	0.035	0.851	2.573	1.155	2.233	0.021	1.421	0.048	0.128	0.976
Ta	0.004	0.015	0.003	0.151	0.000	0.312	0.000	0.005	0.247	1.099	1.113	0.521	0.003	0.343	0.013	0.016	0.079
W	789	1795	2357	2113	2298	2591	1414	2435	1482	2793	3361	3004	2844	2636	2765	3414	2631
Nb	6.99	3.29	6.24	22.98	0.73	29.31	1.32	8.72	21.38	66.80	37.28	32.93	6.55	41.11	6.71	21.38	40.95
Mo	0.023	0.000	0.008	0.000	0.028	0.024	0.000	0.008	0.000	0.000	0.068	0.023	0.051	0.545	0.017	0.009	0.017
Cs	0.057	0.056	0.042	0.052	0.057	0.050	0.051	0.081	0.040	0.050	0.140	0.036	0.047	0.051	0.045	0.051	0.071
Ba	1.105	1.083	1.169	1.080	1.020	1.114	1.065	1.179	0.982	1.085	1.095	1.092	1.207	1.225	1.210	1.107	1.121

cassiterite samples (5-6 ppm Co, 38-42 ppm Ni), while the concentrations of other trace elements are very low (e.g., 5.61 ppm Cu, 0.42 ppm Ga, 1.33 ppm Sr, 0.55 ppm Mo, and 1.23 ppm Ba).

DISCUSSION

Distribution of Trace Elements in Cassiterite

Cassiterite has a tetragonal lattice structure similar to that of rutile, with Sn^{4+} ions in six-fold coordination with oxygen, thus can incorporate a wide range of trace elements, such as Ti, W, Fe, Ta, Nb, U, Mn, V, and Sc (Plimer et al. 1991, Murciego et al. 1997). These elements either displace Sn^{4+} in cassiterite lattice or exist as mineral inclusions (Taylor 1979). In this study, representative time-resolved LA-ICP-MS depth profiles for cassiterite are given in Fig. 5. Most of the measured elements are characterized by a smooth profile, indicating that the samples analyzed are homogeneous and absent of mineral inclusions.

Quadrivalent elements such as Zr, Hf, and Ti can substitute directly for Sn^{4+} in cassiterite without any additional charge balance considerations (Cheng et al. 2019). Nb and Ta in cassiterite exist in the form of 5^{+} ions and enter into the cassiterite lattice by the reactions: $2(Ta, Nb)^{5+}+(Fe, Mn)^{2+}=3Sn^{4+}$ (1) (Möller et al. 1988). Under geological conditions, Sc only occurs in Sc^{3+} valence state, therefore, the positive correlation between V and Sc in cassiterite of the Dalong deposit (Figs. 5b) indicate that V exist as V^{5+} for a charge-balanced coupled substitution of $Sc^{3+} + V^{5+} = 2Sn^{4+}$, and this substitution ($X^{3+} + Y^{5+} = 2Sn^{4+}$ (2)) may occur in cassiterite for many elements (Cheng et al. 2019). If reactions (1) and (2) are the dominant substitution mechanisms for cassiterite, there should be a 2:1 balance between total pentavalent (Nb, Ta) and total divalent (Fe, Mn) cations, and a 1:1 balance between total trivalent (Sc, Fe, Ga) and total pentavalent (V, Nb, Ta) cations. However, in almost all cases, there is a significant excess of trivalent cations (Fig. 4e, f), which means that an additional mechanism is required to incorporate these trivalent cations (mostly Fe^{3+}), for example, the coupled substitution: $Fe^{3+}+OH^{-}=Sn^{4+}+O^{2-}$, as previously proposed (Möller et al. 1988, Tindle & Breaks 1998, Pieczka et al. 2007). Zr-Hf and Nb-Ta have similar ionic radii and ionic charge, thus display similar geochemical behavior and maintain a relatively constant Zr/Hf value of 35 to 40 and an Nb/Ta value of 10 to 20 in most geological systems (Hoskin & Schaltegger 2003, Münker et al. 2003). This may be the main reason for the positive correlation between Zr and Hf as well as Nb and Ta in the Dalong cassiterite samples (Fig. 4c & 4d).

Cathodoluminescence (CL) is an effective means for revealing the complicated microtextures of minerals (Rusk a& Reed 2002). The cathodoluminescence properties of cassiterite largely depend on trace elements' content (Hall & Ribbe 1971, Farmer et al. 1991). Previous research has revealed that Ti and W work as activators, while Fe acts as a quenchant of cassiterite luminescence intensity (Farmer et al. 1991, Wille et al. 2018). Some cassiterite grains in the Dalong tin deposit have clear zonal structures of alternating bright and dark in cathodoluminescence images (Fig. 3f, Fig. 6). The TiO_2 concentration of the annulus is high in the bright band and low in the dark band, and gradually decreases from core to edge, according to electron probe microanalysis (EPMA) (except for slight fluctuations in the bright band) (Fig. 6). The substitution of Sn by Ti is easier to occur at high temperatures (Hu 1988), thus the regular variation characteristics of Ti content may reflect the gradual decrease of ore-forming temperature, and the ore-forming environment is generally relatively stable, but slightly turbulent.

Genesis of Cassiterite

Previous studies have pointed out that elements in cassiterite can be used as indicators of the formation environment

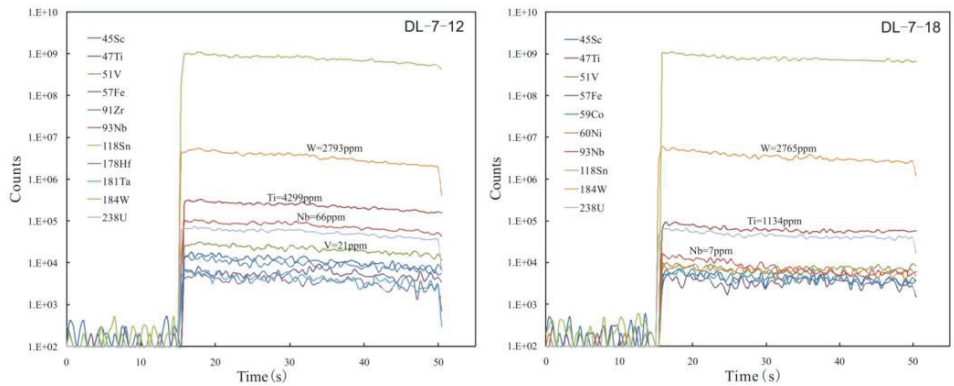

Fig. 5: Representative time-resolved LA-ICP-MS depth profiles for cassiterite from the Dalong deposit.

and ore-forming fluid composition (Schneider et al. 1978, Murciego et al. 1997, Hennigh & Hutchinson 1999). Most of the primary Tin-bearing deposits in the world are magmatic-hydrothermal origin, spatially and genetically related to highly differentiated granite (Taylor 1979, Heinrich & Eadington 1986, Hosking, 1988), and only a few occur as volcanogenic massive sulfide (VMS) deposits or sedimentary-exhalative (SEDEX) deposits, eg., Neves Corvo Cu-Sn VMS deposit (Oliveira et al. 1997), Kidd Creek Cu-Zn-Ag-(Sn) VMS deposit (Hennigh & Hutchinson 1999), and Sullivan Fe-Pb-Zn-(Sn) SEDEX deposit (Hamilton et al. 1982). Cassiterites from granite-related tin deposits display variable colors, while those from SEDEX or VMS deposits are generally colorless (Guo et al. 2018a). In a magmatic-hydrothermal system, the crystallization differentiation of magma will enrich the incompatible elements such as W and Zr in the residual melt, and W can be incorporated into cassiterite by isomorphism or as mineral inclusions, resulting in an increase in the W content of cassiterite in granite-related deposits (Guo et al. 2018b). As for the process of submarine exhalation sedimentation is characterized by low temperature and reduction environment. Under such conditions, the Fe^{2+} is easy to combine with S to form sulfides instead of oxides, leading to low Fe content of cassiterite in the submarine hydrothermal system (Pavlovaer al. 2015). Therefore, cassiterite from granite-related deposits generally contains a larger amount of Fe and W, compared to those from SEDEX/VMS deposits, which provides a method to effectively distinguish the genesis of tin mineralization of these two types. Cassiterites from the Dalong deposit have considerable W contents and relatively high Fe contents and are all plotted in the granite-related tin deposits area in the Fe-W discriminant diagram (Fig. 7a). Cassiterite created in high-temperature systems, such as granites and rare-element pegmatites, is thought to have low Fe and Mn contents and high Nb and Ta contents, as opposed to cassiterite formed in low-temperature hydrothermal environments (Taylor 1979, Tindle & Breaks 1998). Based on this, an Nb-Ta vs Fe-Mn diagram (Fig. 7b) is proposed to trace the genesis of cassiterite (Tindle & Breaks 1998). In this diagram, our data of cassiterite are distributed in the area of the epithermal and hydrothermal deposits, suggesting a magmatic-hydrothermal origin. Furthermore, Chen et al. (2000) put forward that the Mn content of cassiterite decreases significantly with the addition of external hydrothermal fluid, thus, the depletion of Mn in cassiterite from the Dalong deposit may imply the addition of low-temperature fluids during mineralization.

Sources of Sulfur

Sulfur isotopic characteristics can define the formation environment of sulfide and the source of sulfur, which play an important role in inferring the source and forming process of ore deposits (Hoefs 1987, Ohmoto 1997). The $\delta^{34}S$ values of sulfides in the Dalong deposit ($\delta^{34}S$ = 6.88 -10.04) (Xie & Liang 2018), similar to those in Luziyuan deposit ($\delta^{34}S$ = 8.9 - 14.2 ‰) (Xu et al. 2019, Yang et al. 2019), Shuitoushan deposit ($\delta^{34}S$ = 4.1 - 12.2 ‰) (Deng et al. 2017, Zhang et al. 2021), Fangyangshan deposit ($\delta^{34}S$ = 8.24 -14.91) (Xu et al. 2021), Jinchanghe deposit ($\delta^{34}S$ = 2.5 - 11.1‰ (Huang 2014, Li et al. 2019), and Hetaoping deposit ($\delta^{34}S$ = 3.7 - 7.1‰, Chen et al. 2017) in the Baoshan block, range between those of the granite-derived sulfur ($\delta^{34}S$ = –4.0 ~ 9.0‰) (Hoefs

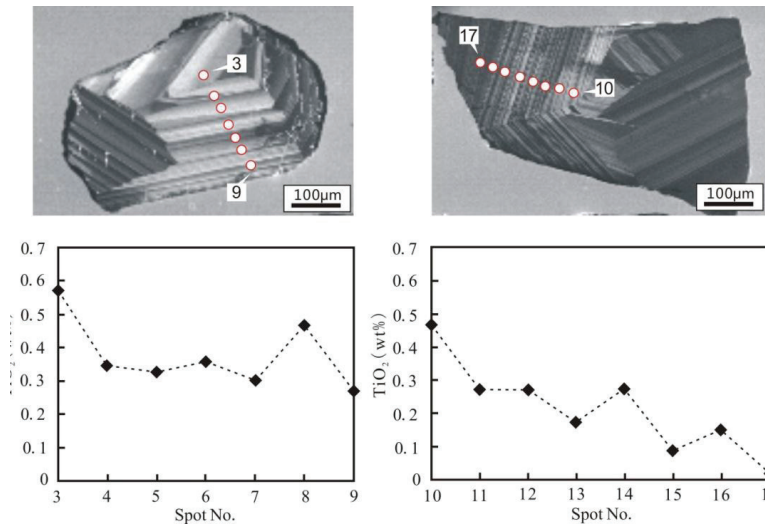

Fig. 6: The zonal structure in the CL image and the compositional variation of cassiterites from the Dalong deposit.

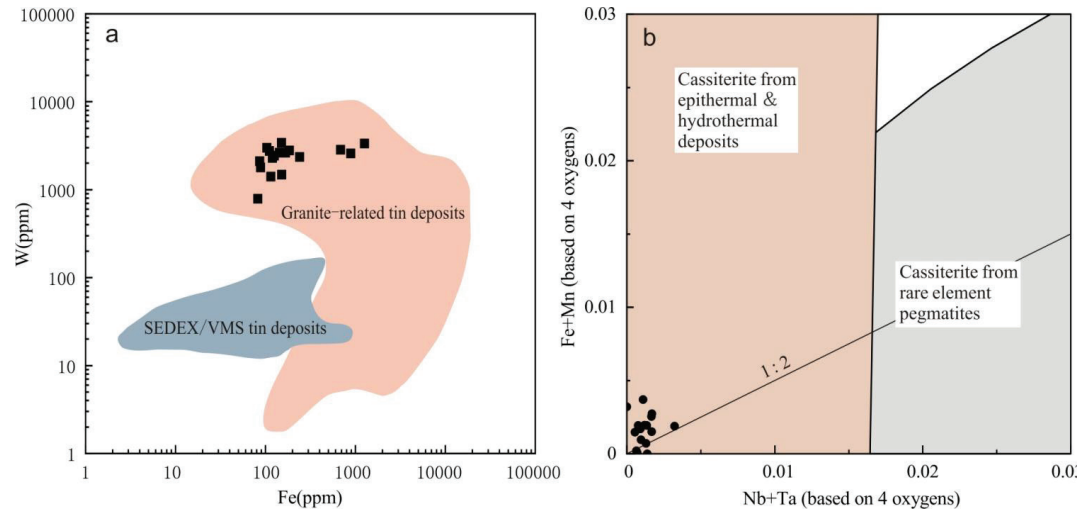

Fig. 7: a. Binary plot of Fe versus W contents in cassiterite from the Dalong deposit (modified from Hennigh & Hutchinson, 1999, Guo et al. 2018a); b. Covariation plot of Nb+Ta with Fe+Mn in cassiterite grains from the Dalong deposit (EPMA data) (modified from Tindle & Breaks 1998, Tan et al. 2018).

1987) and the Cambrian-Triassic seawater sulfate ($\delta^{34}S$ =15.0 ~ 35.0‰) (Claypool et al. 1980) (Fig. 8), suggesting a mixture source of sulfur (Ohmoto 1997). As it is reported that regional concealed intermediate-acid intrusions have been detected at depth under these deposits (reported by Chen et al. 2017, Huang 2014, Liang et al. 2015), a mixed source of sulfur for the Dalong deposit is proposed in this paper, which is initially derived from granite and gradually interfused by seawater during mineralization.

Deposit Type

The orebodies of the Dalong deposit are hosted in calcareous slate, banded micrite limestone, and structural breccia of Upper Cambrian Baoshan formation in vein and lenticular shape, and are strictly controlled by structures. The formation of the deposit is later than the host rock, and the boundary of them is clear, showing typical epigenetic metallogenic characteristics. The mineral composition is simple, mainly composed of cassiterite, pyrite, chalcopyrite, arsenopyrite, quartz, and calcite, associated with correspondingly weak mid-low temperature hydrothermal alterations, such as silicification, pyritization, and sericitization. These geological features are similar to those of typical hydrothermal vein-type tin deposits (Taylor 1979, Hosking 1988, Jiang et al. 2020), suggesting a hydrothermal genesis of the Dalong tin deposit. As discussed above, the trace element composition of cassiterite in Dadong deposits is consistent with that in magmatic-hydrothermal deposits, instead of SEDEX/VMS deposits. The low Mn content of cassiterite and relatively high $\delta^{34}S$ of sulfides indicate that the ore-forming materials originated from deep intermediate-acid intrusions, and maybe gradually interfused by seawater during mineralization. In summary, combined with the geological characteristics of the deposit, the trace element composition of cassiterite, and the sulfur isotope geochemistry of sulfides, the Dagong deposit is supposed to be a magmatic-hydrothermal vein-type tin deposit.

CONCLUSION

(1) The cassiterite is enriched in Fe, W, and Ti, and deplet-

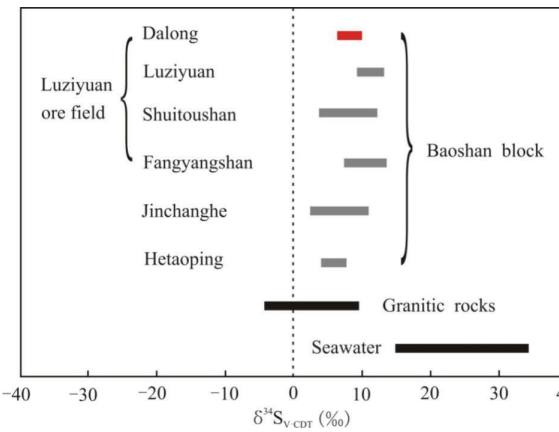

Fig. 8: The sulfur $\delta^{34}S$ values of ore deposits in the Baoshan Block. Data for Dalong deposit are from (Xie & Liang 2018); data for Luziyuan deposit are from (Xu et al. 2019, Yang et al. 2019); data for Shuitoushan deposit are from (Deng et al. 2017, Zhang et al. 2021); data for Fangyangshan deposit are from (Chen 2019); data for Jingchanghe deposit are from (Huang 2014, Li et al. 2019); data for Hetaoping deposit are from (Chen et al. 2017); data for granitic rocks are from (Hoefs 1987); data for seawater are from (Claypool et al. 1980).

ed in Nb, Ta, and Mn, which indicate that the Dalong deposit was formed in a granite-related magmatic-hydrothermal system.

(2) The similar sulfur isotopic characteristics of the Dalong tin deposit and the Luziyuan, Shuitoushan, and Fangyangshan deposits in the Luziyuan ore field indicate that they have similar sources of sulfur, which is originally derived from the concealed intermediate-acid intrusions in deep and then mixed by seawater during mineralization.

(3) The Dalong tin deposit belongs to a magmatic-hydrothermal vein-type deposit in genesis. The concealed intermediate-acid intrusions provide the most important ore-forming fluid and metallogenic materials for mineralization.

ACKNOWLEDGMENTS

This work was supported by the Yunnan Fundamental Research Projects (2019FD065, 2019FA018), Commonwealth Project from Yunnan Science and Technology Award – Outstanding Contribution Award (2017001), Yunnan University "Donglu Young and Middle-aged Key Teachers" Training Program (C176220200), Scientific research fund project of Education Office of Yunnan Province (2021J0001).

REFERENCES

Chen, F., Deng, J., Shu, Q., Li, G., Cui, X., Zhao, F. and Wang, Q. 2017. Geology, fluid inclusion, and stable isotopes (O, S) of the Hetaoping distal skarn Zn-Pb deposit, northern Baoshan block, SW China. Ore Geol. Rev., 90: 913-927.

Chen, F., Li, X., Wang, X., Li, Q. and Siebel W. 2007. Zircon age and Nd – Hf isotopic composition of the Yunnan Tethyan belt, Southwestern China. Int. J. Earth Sci., 96(6): 1179-1194.

Chen, J., Wang, R.C., Zhou, J.P. and Ji, J.F. 2000. The geochemistry of Tin. Nanjing University Press, Nanjing, pp 1-320 (in Chinese with English abstract)

Chen, L., Ni, P., Dai, B., Li, W., Chi, Z. and Pan J. 2019. The genetic association between Quartz Vein- and Greisen-Type mineralization at the Mapping W – Sn deposit, Southern Jiangxi, China: Insights from zircon and cassiterite U – Pb ages and cassiterite trace element composition. Minerals, 9(7): 411.

Cheng, H.L., Xiang, H.L. and Yang, S. 2006. Geological characteristics of Dalong tin polymetallic deposit in Yunnan and its exploration prospective. Mineral Resour. Geol., 03: 255-259 (in Chinese with English abstract)

Cheng, Y., Spandler, C., Kemp, A., Jingwen, M.J., Rusk, B., Hu, Y. and Blake, K. 2019. Controls on cassiterite (SnO2) crystallization; evidence from cathodoluminescence, trace-element chemistry, and geochronology at the Gejiu tin district. Am. Mineral., 104(1): 118-129

Claypool, G.E., Holser, W.T., Kaplan, I.R., Sakai, H. and Zak, I. 1980. The age curves of sulfur and oxygen isotopes in marine sulfate and their mutual interpretation. Chem. Geol., 28: 199-260.

Deng, J., Wang, Q., Li, G. and Santosh, M. 2014. Cenozoic tectonic-magmatic and metallogenic processes in the Sanjiang region, Southwestern China. Earth Sci. Rev., 138: 268-299.

Deng, M.G, Zhao, J.X., Liu, F.X., Yu, H.J. and Sun, B.D. 2017. Discussion on sources of metallogenic fluids and materials of the Shuitoushan Pb-Zn deposit in Zhenkang, western Yunnan: Evidence from H, O, S and Pb isotopes. Acta Petrol. Sin., 33: 2001-2017. (in Chinese with English abstract)

Dong, M., Dong, G., Mo, X., Santosh, M., Zhu, D., Yu, J., Nie, F. and Hu, Z. 2013. Geochemistry, zircon U – Pb geochronology and Hf isotopes of granites in the Baoshan Block, western Yunnan: Implications for early paleozoic evolution along the Gondwana margin. Lithos, 179: 36-47.

Farmer, C.B., Searl, A. and Halls, C. 1991. Cathodoluminescence and growth of cassiterite in the composite lodes at South Crofty Mine, Cornwall, England. Mineral. Mag., 55(380): 447-458.

Fei, G.C., Menuge, J., Li, Y.Q., Yang, J.Y., Deng Y., Chen, C.S., Yang, Y.F., Yang, Z., Qin, L.Y., Zheng, L. and Tang, W.C. 2020. Petrogenesis of the Lijiagou spodumene pegmatites in Songpan-Garze Fold Belt, West Sichuan, China: Evidence from geochemistry, zircon, cassiterite, and coltan U-Pb geochronology and Hf isotopic compositions. Lithos, 364-365.

Gemmrich, L., Torró L., Melgarejo, J.C., Laurent, O., Vallance, J., Chelle-Michou, C. and Sempere, T.P.A. 2021. Trace element composition and U-Pb ages of cassiterite from the Bolivian tin belt, Mineralium Deposita. HAL Open Sci., 36: 1-64.

Guo, J., Zhang, R., Li, C., Sun, W., Hu, Y., Kang, D. and Wu, J. 2018a. The genesis of the Gaosong Sn–Cu deposit, Gejiu district, SW China: Constraints from in situ LA-ICP-MS cassiterite U – Pb dating and trace element fingerprinting, Ore Geol. Rev., 92: 627-642.

Guo, J., Zhang, R., Sun, W., Ling, M., Hu, Y., Wu, K., Luo, M. and Zhang, L. 2018b, Genesis of tin-dominant polymetallic deposits in the Dachang district, South China: Insights from cassiterite U – Pb ages and trace element compositions. Ore Geol. Rev., 95: 863-879.

Hall, M.R. and Ribbe, P.H. 1971. An electron microprobe study of luminescence centers in cassiterite. Am. Mineral., 56: 31-45.

Hamilton, J.M., Bishop, D.T., Morris, H.C. and Owens, O.E. 1982. Geology of the Sullivan Orebody, Kimberley, B.C., Canada,

Hennigh, Q. and Hutchinson R. 1999. Cassiterite at Kidd Creek: An example of volcanogenic massive sulfide-hosted tin mineralization. Econ. Geol., 61: 431-440.

Hoefs, J.S. (ed). 1987. Stable isotope geochemistry. 3rd edition. Spring Verlag, Berlin, Germany, pp.1-250.

Hoskin, P.W.O. and Schaltegger, U. 2003, The composition of zircon and igneous and metamorphic petrogenesis. Rev. Mineral. Geochem., 53(1): 27-62.

Hosking, K. (ed). 1988. The World's Major Types of Tin Deposit: Geology of Tin Deposits in Asia and the Pacific,

Hu, Z.N. 1988. Typomorphic characteristics of cassiterite in the Yunlong Tin Deposit, Yunnan Province. Acta Mineral. Sin., (04): 381-384 (in Chinese with English abstract)

Huang, H. 2014. The Research on Geological Characteristics and Metallogenesis of the Jinchanghe Fe-Cu-Pb-Zn Polymetallic Deposit, Yunnan Province. China University of Geosciences, Beijing, pp.1-95 (in Chinese with English abstract)

Jiang, C.X., Lu, Y.X., Chen, Y.Q., Yang, S.S., Zhou, D. and Yu, H.J. 2013. Metallogenic model and integrated prospecting pattern of the Luziyuan Pb-Zn polymetallic deposit, southwestern Yunnan Province. Geol. Bull. China, 32(11): 1832–1844.

Jiang, S., Yu, J. and Lu, J. 2004. Trace and rare-earth element geochemistry in tourmaline and cassiterite from the Yunlong tin deposit, Yunnan, China: implication for migmatitic–hydrothermal fluid evolution and ore genesis. Chem. Geol., 209(3-4): 193-213.

Jiang, S.Y., Zhao, K.D., Jiang, H., Su H.M., Xiong S.F. 2020, Spatiotemporal distribution, geological characteristics and metallogenic mechanism of tungsten and tin deposits in China: An overview, Chin Sci Bull, 65(33): 3730-3745 (in Chinese with English abstract)

Li, G., Wang, Q., Huang, Y., Chen, F. and Dong P. 2015. Discovery of Hadean−Mesoarchean crustal materials in the northern Sibumasu block and its significance for Gondwana reconstruction. Precamb. Res., 271: 118-137.

Li, Z.H., Liu, X.L., Chen, J.H., Luo, Y., Zhang, C.Z. and Wang, S.S. 2019. S-Pb isotopic characteristics of Jinchanghe iron-copper-lead-zinc polymetallic deposit in Baoshan City, Yunnan province. J. Geomech., 25(S1): 115-118 (in Chinese with English abstract)

Liang, S., Jiao, Y. and Guo J. 2015. Prediction of hidden granites in the Luziyuan Area of Yunnan Province and the prospecting direction. Acta Geol. Sin., 89(5): 1781-1782.

Liao, S.Y., Wang, D., Tang Y., Yin F., Cao, S., Wang, L., Wang, B. and Sun, Z. 2015. Late Paleozoic Woniusi basaltic province from Sibumasu terrane: Implications for the breakup of eastern Gondwana's northern margin.. Geol. Soc. Am. Bull., 127(9-10): 1313-1330.

Liu, S., Hu, R., Gao, S., Feng, C., Huang, Z., Lai, S., Yuan, H., Liu, X., Coulson, I.M., Feng, G., Wang, T. and Qi, Y. 2009. U − Pb zircon, geochemical and Sr−Nd − Hf isotopic constraints on the age and origin of early Palaeozoic I-type granite from the Tengchong − Baoshan Block, Western Yunnan Province, SW China. J. Asian Earth Sci., 36(2): 168-182.

Liu, S., Liu, Y., Ye, L., Wei, C., Cai, Y. and Chen, W. 2021. The genesis of Dulong Sn-Zn-in polymetallic deposit in Yunnan Province, South China: Insights from cassiterite U-Pb ages and trace element compositions. Minerals, 11(2): 199.

Metcalfe, I. 2011. Gondwana dispersion and Asian accretion: Tectonic and palaeogeographic evolution of eastern Tethys. J. Asian Earth Sci., 66: 1-33.

Möller, P., Dulski, P., Szacki, W., Malow, G. and Riedel, E. 1988. Substitution of tin in cassiterite by tantalum, niobium, tungsten, iron and manganese. Geochim. Et Cosmoch. Acta, 52(6): 1497-1503.

Münker, C., Pfänder, J.A., Weyer, S., Büchl, A., Kleine, T. and Mezger, K. 2003. Evolution of planetary cores and the earth-moon system from Nb/Ta systematics. Sci. Am. Assoc. Adv. Sci., 301(5629): 84-87.

Murciego, A., Garcla Sanchez, A., Dusausoy, Y., Martin Pozas, J.M. and Ruck R. 1997. Geochemistry and EPR of cassiterites from the Iberian Hercynian Massif. Mineral. Mag., 61(406): 357-365.

Nie, F., Dong, G.C., Mo, X.X., Zhu, D.C., Dong, M.L. and Wang, X. 2012. Geochemistry, zircon U-Pb chronology of the Triassic granites in the Changning-Menglian suture zone and their implications. Acta Petrol. Sin., 28: 1465-1476 (in Chinese with English abstract)

Ohmoto, H.G.M.B.. 1997. Sulfur and Carbon Isotopes[A]. In: Barnes, H. L. (ed.), Geochemistry of Hydrothermal Ore Deposits[C]. 3rd Edition. John Wiley and Sons., New York, pp. 65-112.

Oliveira, J.T., Pacheco, N., Carvalho, P. and Ferreira A. (eds.). 1997. The Neves Corvo Mine and the Paleozoic Geology of Southwest Portugal: In Barriga, F.J.A.S. and Carvalho, D. (eds.), Geology and VMS Deposits on the Iberian Pyrite Belt. Society of Economics Geologists, Lisbon, pp. 422-436.

Pavlova, G.G., Palessky, S.V., Borisenko, A.S., Vladimirov, A.G., Seifert, T. and Phan, L.A. 2015. Indium in cassiterite and ores of tin deposits. Ore Geol. Rev., 66: 99-113.

Pieczka, A., Gołębiowska B. and Parafiniuk, J. 2007. Geochemistry and origin of the cassiterite from Rędziny, Lower Silesia, Poland. Mineralogia, 38(2): 219-230.

Plimer, I.R., Lu, J. and Kleeman, J.D. 1991. Trace and rare earth elements in cassiterite sources of components for the tin deposits of the Mole Granite, Australia. Mineral. Dep., 26(4): 73.

Rusk, B. and Reed, M. 2002. Scanning electron microscope-cathodoluminescence analysis of quartz reveals complex growth histories in veins from the Butte porphyry copper deposit, Montana. Geology, 30(8): 727-730.

Schneider, H.J., Dulski, P., Luck, J.M., Ller, P. and Villalpando, A. 1978. Correlation of trace element distribution in cassiterites and geotectonic position of their deposits in Bolivia. Mineral. Dep. 13(1): 54-65.

Tan, S.C., Guo, X.Y., He, X.H. and Xie, Z.P. 2018. Mineral chemical characteristics and genesis of cassiterite in Gejiu Tin-Polymetallic deposit, Yunnan Province. J. Jilin Univ. Earth Sci. Edn., 48(03): 736-753 (in Chinese with English abstract)

Tao, Y., Hu, R.Z., Zhu, F. L., Ma, Y. S., Ye, L. and Cheng, Z.T. (2010). Ore-forming age and the geodynamic background of the Hetaoping lead-zinc deposit in Baoshan, Yunnan. Acta Petrol. Sin., 26: 1760-1772 (in Chinese with English abstract)

Taylor, R.G. (ed.). 1979. Geology of Tin Deposits. Elsevier Scientific Pub. Co, New York.

Tindle A.G. and Breaks, F.W. 1998. Oxide minerals from the Separation Rapids rare-element granitic pegmatite group, Northwestern Ontario. Canad. Mineral., 36(2): 609-635.

Wang, Q., Deng, J., Li, C., Li, G., Yu, L. and Qiao, L. 2014a. The boundary between the Simao and Yangtze blocks and their locations in Gondwana and Rodinia: Constraints from detrital and inherited zircons. Gondwana Res., 26(2): 438-448.

Wang, Z.Q., Chen, B. and Ma, X. H. 2014b. In situ LA-ICP-MS U-Pb age and geochemical data of cassiterite of the Furong tin deposit, the Nanling Range: Implications for the origin and evolution of the ore-forming fluid, China Sci. Bull., 59(25): 2505-2519 (in Chinese with English abstract)

Xie, J.M. and Liang, Q. L. 2018. Study on geological characteristics and prospecting indicator of Dalong Sn mining area in Yunnan Province. China Metal Bull., (09): 34-35. (in Chinese)

Xu, R., Chen, W., Deng, M., Li, W., Chen, F., Lai, C., Sha, J., Jia, Z. and Liu, W. 2021. Geology and C-O-S-Pb isotopes of the Fangyangshan Cu-Pb-Zn deposit in the Baoshan block (SW China): Implications for metal source and ore genesis. Ore Geol. Rev., 132: 103992.

Xu R., Li, W., Deng, M., Zhou, J., Ren, T. and Yu, H. 2019. The genesis of the superlargeLuziyuan Zn-Pb-Fe(-Cu) distal skarn deposit in western Yunnan (SW China): Insights from ore geology and C-H-O-S isotopes. Ore Geol. Rev., 107: 944-959.

Yang, Y., Ye, L., Bao, T., Gao, W. and Li, Z. 2019. Mineralization of Luziyuan Pb − Zn skarn deposit, Baoshan, Yunnan Province, SW China: evidence from petrography, fluid inclusions, and stable isotopes. Geol. Mag., 156(4): 639-658.

Ye, L., Gao, W., Cheng, Z., Yang, Y. and Tao Y. 2010. LA-ICP-MS Zircon U-Pb geochronology and petrology of the Muchang Alkali Granite, Zhenkang County, Western Yunnan Province, China. Acta Geol. Sin., 84(6): 1488-1499.

Zhang, C.Y., Li, W.C., Yu, H.J. and Li, W.T. 2021. The genesis of the Shuitoushan Pb − Zn deposit, Baoshan Block, Sanjiang region: Constraints from fluid inclusions and O, S, Pb isotopes. Geol. J., 65: 111-121.